

# “Cross” Supermicelles via the Hierarchical Assembly of Amphiphilic Cylindrical Triblock Comicelles

Xiaoyu Li,<sup>†,||,§</sup> Yang Gao,<sup>†,§</sup> Charlotte E. Boott,<sup>†</sup> Dominic W. Hayward,<sup>†</sup> Robert Harniman,<sup>†</sup> George R. Whittell,<sup>†</sup> Robert M. Richardson,<sup>‡</sup> Mitchell A. Winnik,<sup>⊥</sup> and Ian Manners<sup>\*,†</sup>

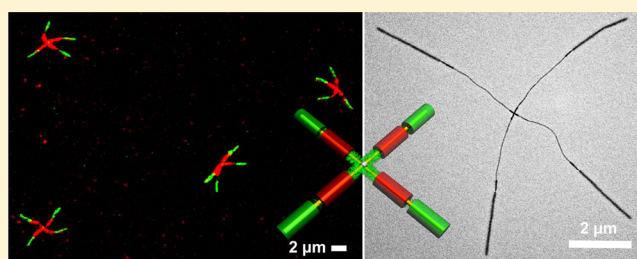
<sup>†</sup>School of Chemistry, University of Bristol, Bristol BS8 1TS, United Kingdom

<sup>‡</sup>School of Physics, University of Bristol, Bristol BS8 1TS, United Kingdom

<sup>⊥</sup>Department of Chemistry, University of Toronto, Toronto, Ontario M5S 3H6, Canada

## Supporting Information

**ABSTRACT:** Self-assembled “cross” architectures are well-known in biological systems (as illustrated by chromosomes, for example); however, comparable synthetic structures are extremely rare. Herein we report an in depth study of the hierarchical assembly of the amphiphilic cylindrical P–H–P triblock comicelles with polar (P) coronal ends and a hydrophobic (H) central periphery in a selective solvent for the terminal segments which allows access to “cross” supermicelles under certain conditions. Well-defined P–H–P triblock comicelles M(PFS-*b*-PtBA)-*b*-M(PFS-*b*-PDMS)-*b*-M(PFS-*b*-PtBA) (M = micelle segment, PFS = polyferrocenyldimethylsilane, PtBA = poly(*tert*-butyl acrylate), and PDMS = polydimethylsiloxane) were created by the living crystallization-driven self-assembly (CDSA) method. By manipulating two factors in the supermicelles, namely the H segment-solvent interfacial energy (through the central H segment length,  $L_1$ ) and coronal steric effects (via the PtBA corona chain length in the P segment,  $L_2$  related to the degree of polymerization  $DP_2$ ) the aggregation of the triblock comicelles could be finely tuned. This allowed a phase-diagram to be constructed that can be extended to other triblock comicelles with different coronas on the central or end segment where “cross” supermicelles were exclusively formed under predicted conditions. Laser scanning confocal microscopy (LSCM) analysis of dye-labeled “cross” supermicelles, and block “cross” supermicelles formed by addition of a different unimer to the arm termini, provided complementary characterization to transmission electron microscopy (TEM) and dynamic light scattering (DLS) and confirmed the existence of these “cross” supermicelles as kinetically stable, micron-size colloiddally stable structures in solution.



## INTRODUCTION

Amphiphilic molecular species are ubiquitous in both the natural world and everyday life, and typical examples include phospholipids in cell membranes and surfactant molecules in detergents. These species are composed of a hydrophilic headgroup and a short hydrophobic segment and can self-organize into micellar aggregates in water.<sup>1</sup> Amphiphilic block copolymers (BCPs), higher molar mass analogues of these molecular amphiphiles, can also self-assemble in selective solvents.<sup>2</sup> Because of the enhanced hydrophobic effect arising from the longer hydrophobic blocks, BCP micelles are generally formed at a much lower concentration. Moreover, as intermicellar unimer (molecularly dissolved BCP) exchange is much slower or nonexistent, kinetically stable nonequilibrium morphologies are accessible in addition to the thermodynamically preferred spherical, cylindrical and vesicular aggregates.<sup>3</sup>

“Supermicelles” are micron size hierarchical structures constructed from BCP micelle building blocks, and these assemblies have barely been explored until recently.<sup>4</sup> In 2003 spherical micelles with patches of different polarity were self-assembled into supermicelles consisting of small aggregates.<sup>5</sup>

This work has been extended to yield a range of remarkable linear and branched segmented structures.<sup>6</sup> The assembly of patchy BCP micelles into large supermicelles,<sup>7</sup> nanotubes and nanosheets<sup>8</sup> has also been demonstrated. Shell-cross-linked spherical BCP micelles have also been electrostatically assembled on cylinders of opposite coronal charge.<sup>9</sup> The resulting sphere-cylinder supermicelles undergo cell internalization, unlike the uncoated, charged cylindrical precursors. Such hybrid supermicelles can simultaneously deliver gene-silencing RNA and provide an imaging capability through radiolabeling, offering potential for theranostic applications in biomedicine.<sup>9</sup> Supermicelles can also be prepared by connecting two micellar species via covalent bonds.<sup>10</sup>

We recently reported a facile, solution-phase route to prepare amphiphilic cylindrical micelles,<sup>11</sup> based on living crystallization-driven self-assembly (CDSA), as an alternative route to patchy nanoparticles.<sup>12</sup> This method allows the formation of monodisperse samples of cylinders possessing segmented

Received: December 6, 2015

Published: February 15, 2016

coronal regions of precisely controlled length and with distinct chemistries via the epitaxial growth of added BCP unimers with a crystallizable core-forming block from the termini of seed micelles.<sup>11,13</sup> Such amphiphilic block comicelles are able to self-assemble either side-by-side or end-to-end in selective solvents to form hierarchical structures on the 1–100  $\mu\text{m}$  length scale, such as spherical and cylindrical supermicelles or extended 1D or 3D structures, respectively.<sup>11c</sup>

Self-assembled structures with “cross” architectures are well-known in biology (e.g., chromosomes), whereas comparable synthetic constructs are extremely rare. With this in mind, we have recently shown that the hierarchical self-assembly of triblock comicelles with central blocks bearing either hydrogen-bond donor or acceptor groups are capable of forming “cross” supermicelles.<sup>14</sup> Such structures were also generated from triblock comicelles in polar media by the use of hydrophobic central segments. The coronal chains present in the solvophobic central segments of the supermicelles can also be cross-linked,<sup>15</sup> thereby allowing further stabilization of the “cross” architectures. This facilitates the creation of highly complex structures such as “windmill” micelles by the application of further living CDSA steps.<sup>14</sup> However, despite their interesting potential, the conditions under which “cross” supermicelles are formed relative to other assemblies were not studied.

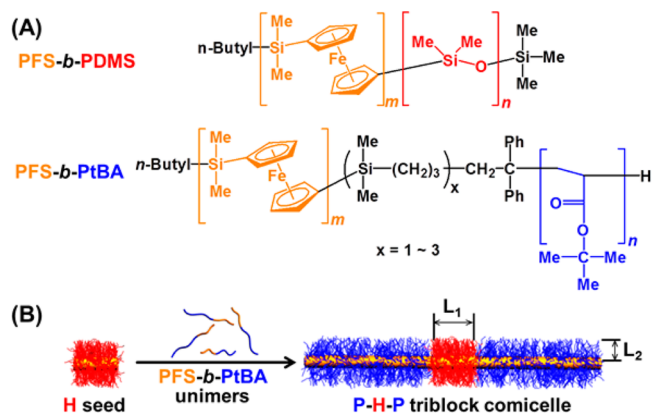
In this paper we report a systematic and detailed study on the self-assembly of amphiphilic, centrosymmetric cylindrical P–H–P triblock comicelles with a hydrophobic (H) central segment and polar (P) segments at the termini in selective solvents. We show that by controlling two key parameters, namely the central H segment length and the corona chain length in the P segment, the aggregation behavior of the triblock comicelles can be understood. We construct a phase diagram that allows “cross” supermicelles to be exclusively formed under predictable conditions. We also demonstrate that the approach can be applied to different block comicelle systems.

## RESULTS

**1. Design, Synthesis, and Characterization of Amphiphilic P–H–P Triblock Comicelles.** For the systematic study of the triblock comicelle assembly, two kinds of BCPs were used (Scheme 1(A)): an H (hydrophobic and insoluble in a polar solvent) segment-forming BCP PFS-*b*-PDMS (PFS = polyferrocenyldimethylsilane, PDMS = polydimethylsiloxane) and a series of the P (polar, soluble in a polar solvent) segment-forming BCPs PFS-*b*-PtBA (PtBA = poly(*tert*-butyl acrylate)), which contain similar PFS block lengths and different PtBA chain lengths (Table S1). The BCPs were prepared by sequential living anionic polymerization of dimethylsila[1]-ferrocenophane and hexamethylcyclotrisiloxane or *tert*-butyl acrylate, respectively.<sup>16</sup> And all contain a crystallizable PFS core-forming block.<sup>17</sup>

For convenience, as the crystalline PFS core was a common feature, all of the micelles are depicted in an abbreviated form that reflects their coronal chemistry (for example, triblock comicelle M(PFS-*b*-PtBA)-*b*-M(PFS-*b*-PDMS)-*b*-M(PFS-*b*-PtBA), is described as P–H–P. These cylinders were prepared by seeded growth from short H cylindrical micelles (seeds) via living CDSA (Scheme 1(B)). First, monodisperse H micelle seeds were prepared by adding PFS<sub>28</sub>-*b*-PDMS<sub>560</sub> unimers in THF to a solution of small PFS<sub>28</sub>-*b*-PDMS<sub>560</sub> crystallites<sup>13c</sup> (ca. 16 nm in length) in hexane, and the length was controlled by

**Scheme 1.** (A) Chemical Structures of PFS-*b*-PDMS and PFS-*b*-PtBA Diblock Copolymers, Abbreviated as H and P, Respectively; (B) The CDSA Process to Prepare a P–H–P Triblock Comicelle and the Definition of  $L_1$  and  $L_2$ <sup>a</sup>



<sup>a</sup>Orange, red and blue chains represent PFS, PDMS and PtBA, respectively.

the ratio of the PFS<sub>28</sub>-*b*-PDMS<sub>560</sub> unimers to the small crystallites (see Table S2). To the seed solution, in a solvent mixture of *n*-hexane:isopropanol (*i*-PrOH) = 1:4, v/v, in which both PtBA and PDMS chains were soluble, the desired amount of PFS-*b*-PtBA unimers in a small portion of THF was added to achieve the targeted cylinder length. All the seed cylinders and triblock comicelles were characterized by transmission electron microscopy (TEM) and the results are summarized in Figure S1. As can be appreciated from the images and data (Table S2 and Table S3), both seeds and triblock comicelles were uniform in length, due to the control arising from the living CDSA method. This ensured that all the micelles from the sample possessed very similar amphiphilicity, a feature likely to facilitate their controlled hierarchical assembly.

The hierarchical self-assembly of the P–H–P triblock comicelles is expected to depend on the relative dimensions of the segments present. To consider this in more detail, we define the length of the central H segments of the block comicelle building blocks as  $L_1$ , and the length of soluble corona chains (or corona layer thickness) in the terminal P segments as  $L_2$  (Scheme 1(B) right).

$L_1$  is the length of the H micelle seeds, from which the triblock comicelles are grown, and thus the values of  $L_1$  can be obtained from the TEM images of the seed micelles.  $L_2$  is more challenging to determine. However, the value will be dependent on the degree of polymerization (DP) of the PtBA chains in the PFS-*b*-PtBA BCP (see SI pages S8–S9 for a discussion on the precise relationship between  $L_2$  and DP).<sup>18</sup> In this work, where we are interested in a qualitative approach to understanding the hierarchical self-assembly, we have therefore directly used the value of the degree of polymerization of PtBA, represented as DP<sub>2</sub>, as a replacement for  $L_2$  (for example, for a P segment from PFS<sub>20</sub>-*b*-PtBA<sub>170</sub>, DP<sub>2</sub> = 170). To determine the value of DP<sub>2</sub> for the diblock copolymer PFS-*b*-PtBA, the DP of the PFS homopolymer was obtained first by MALDI-TOF analysis and subsequently the DP<sub>2</sub> was calculated based on the results from <sup>1</sup>H NMR integration for the diblock copolymer.

When the P–H–P triblock comicelles are dispersed in a polar solvent we anticipate that, at least to a first approximation, the value of  $L_1$  will determine the interfacial energy between the insoluble short H segments and the solvent. To minimize the H

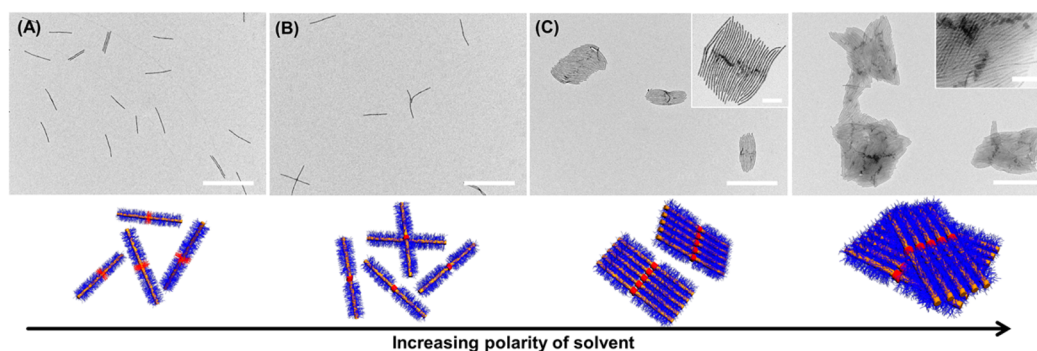


**Figure 1.** TEM images of P–H–P triblock comicelles with  $L_1 = 16$  nm,  $DP_2 = 170$  in (A) *n*-hexane:*i*-PrOH = 1:4; (B) *i*-PrOH; (C) *i*-PrOH:MeOH = 5:5 and (D) MeOH. Scale bars are 1  $\mu$ m and those for the insets are 200 nm.

segment/solvent interfacial energy, the triblock comicelles would be expected to aggregate and form large bundles. On the other hand, the value of  $L_2$  (or  $DP_2$ ) would be expected to characterize a counterbalancing steric effect from the solvated coronas of the P segments, which would tend to hinder aggregation. The relative counterbalancing of these two effects would be expected to give rise to a variety of aggregate morphologies, as revealed in practice in the studies described below.

**2. Self-Assembly of Amphiphilic P–H–P Triblock Comicelles in Selective, Polar Solvents.** To study the self-assembly of the P–H–P amphiphilic comicelles in selective solvents, we started with the P–H–P triblock comicelles with  $L_1 = 16$  nm and  $DP_2 = 170$  dispersed in *n*-hexane:*i*-PrOH (1:4, v/v). The solution was subsequently dialyzed into *i*-PrOH over 1 day and MeOH over 3 days. As both *i*-PrOH and MeOH are poor solvents for PDMS chains, aggregation of the H segments leads to the formation of discrete or aggregated supermicelles in order to minimize the interfacial energy.

TEM analysis (Figure 1) suggested that the degree of aggregation of the triblock comicelles increased as the polarity of the solvent mixture increased. When the block comicelles were dialyzed into *i*-PrOH, mainly individual triblock comicelles and occasional “cross”-shaped supermicelles (formed by the aggregation of two cylinders at the H segments) were observed (Figure 1(B)). When the solvent became more polar (from *i*-PrOH to MeOH), the comicelles formed small bundles initially (*i*-PrOH:MeOH = 5:5, Figure 1(C)), with the H segments well aligned inside the bundles. Eventually these small bundles aggregated further to form three-dimensional aggregates (MeOH, Figure 1(D)). From this set of experiments, it could be concluded that the degree of aggregation was related to the solvent quality and the resulting interfacial tension. Thus, to simplify the subsequent studies, we focused on the self-assembly behavior of the triblock comicelles in MeOH, in which they show the most extensive aggregation.

**3. Influence of  $L_1$  and  $DP_2$  on Supermicelle Architecture.** To study the influence of  $L_1$  and  $DP_2$  on the self-assembly of triblock comicelles, two sets of experiments were carried out. In the first set, P–H–P triblock comicelles with four different  $L_1$  values, 16, 27, 37, and 56 nm (Table S3) and the same value of  $DP_2$ , 280, were dialyzed into MeOH and the resulting aggregates were studied by TEM. When  $L_1 = 16$  nm, the triblock comicelles formed “cross”-shaped supermicelles (Figure 2(A)) with only two micelles aggregated together through the central H segments. When the  $L_1$  value increased, the hydrophobic effect from the H segments was

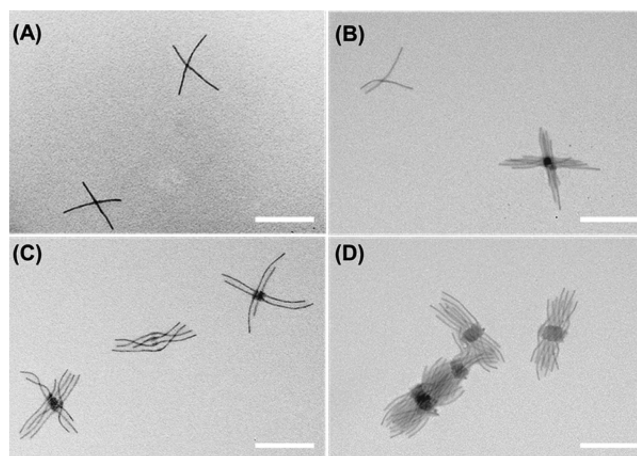


**Figure 2.** TEM images of triblock comicelles P–H–P in MeOH with  $DP_2 = 280$  and  $L_1 =$  (A) 16 nm; (B) 27 nm; (C) 37 nm; (D) 56 nm. Scale bars are 500 nm.

enhanced, and thus multiple “cross” (Figure 2(B)), mixed multiple “cross” and bundles (Figure 2(C)), and eventually bundles of triblock comicelles (Figure 2(D)) were formed. Because of the aggregation of insoluble PDMS chains, the dense supermicelle core regions arising from the central H segments appeared darker by TEM.

In the second set of experiments, we fixed  $L_1$  to 27 nm and investigated amphiphilic triblock comicelles with four different  $DP_2$  values ( $DP_2 = 600, 460, 280$  and  $170$ , the characteristics are shown in Table S3). After dialysis of the triblock comicelle samples into MeOH, in the case where  $DP_2 = 600$ , the triblock comicelles still remained as individual structures and no aggregation could be observed (Figure 3(A)). However, when  $DP_2$  was decreased to 460 and 280, multiple “cross” supermicelles were observed (Figure 3(B, C)), and large three-dimensional bundles appeared when  $DP_2$  was further reduced to 170 (Figure 3(D)).

From those two sets of experiments it can be concluded that the aggregation of the triblock comicelles can be enhanced via either a stronger hydrophobic interaction (through a larger H segment-solvent interfacial energy from increasing the  $L_1$  value), or a reduced coronal steric repulsion effect (from a smaller  $DP_2$  value). However, to more fully explore the influence of  $L_1$  and  $DP_2$  on the supermicellar structures formed by the triblock comicelles, a more systematic study was performed (see Section 4 below).

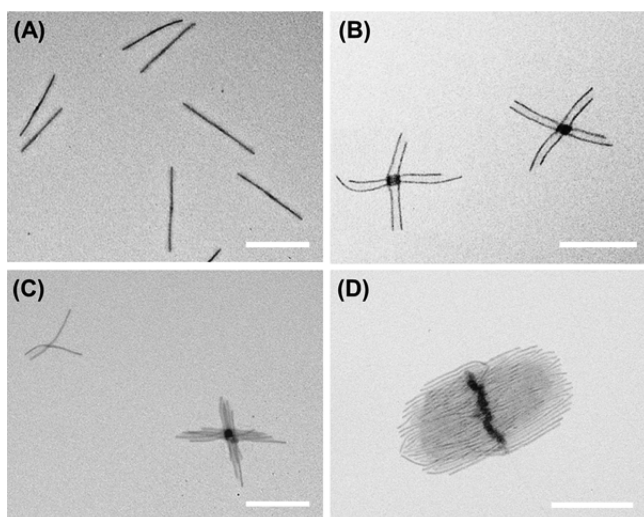


**Figure 3.** TEM images of P–H–P triblock comicelles in MeOH with  $L_1 = 27$  nm and  $DP_2 =$  (A) 600; (B) 460; (C) 280; and (D) 170. Scale bars are 500 nm.

First, we addressed an important assumption that has been made in the interpretation of the data. Namely, that the supermicellar structures are formed in solution rather than on drying during the TEM sample preparation. Several samples were therefore characterized in solution by dynamic light scattering (DLS). As shown in Figure 4(E), in comparison with the individual cylindrical block comicelles (Figure 4(A)), the multiple “cross” micelles (Figure 4(B)) showed a negligible difference in apparent hydrodynamic diameter ( $D_{h,app}$ ), but the cylinder bundles (Figure 4(C)) showed a much larger  $D_{h,app}$ . This appears to be reasonable, as the hydrodynamic radius of the “cross” micelles would be expected to be very similar to that of the individual cylindrical triblock comicelle components, whereas the larger bundles possessed many more cylinders as part of their structure, and therefore a larger hydrodynamic size would be anticipated.

Unfortunately, the very large aggregates (Figure 4(D)) were too large to be characterized by DLS. Thus, optical transmittance measurements on the solution were performed. As shown in Figure 4(F), the solution with very large aggregates showed significantly reduced transmittance relative to those with multiple “cross” supermicelles or with small bundles. The combination of DLS and optical transmittance results clearly suggests that these aggregates form from the triblock comicelles prior to solvent evaporation. Further, conclusive evidence, in the form of laser scanning confocal microscopy analysis, is presented below (Section 6).

Before proceeding with a systematic study we also wanted to confirm that the observed aggregation in MeOH was solely induced by the collapse of PDMS chains in the corona of the central block and that the coronal PtBA chains of the adjoining terminal segments play no significant role. To address this issue, we explored whether cylindrical micelles from the diblock copolymer PFS-*b*-PtBA alone will form similar aggregates in MeOH. As the triblock comicelles with  $L_1 = 16$  nm and  $DP_2 = 600$  did not form aggregates in MeOH, this suggested that long PtBA corona chains do not induce aggregation between the triblock comicelles. For confirmation, we also investigated the behavior of cylindrical homomicelles ( $L_n = 510$  nm,  $L_w/L_n = 1.14$ ) prepared from PFS<sub>20</sub>-*b*-PtBA<sub>170</sub> diblock copolymer. As shown in Figure S3, these cylinders appear well-dispersed in

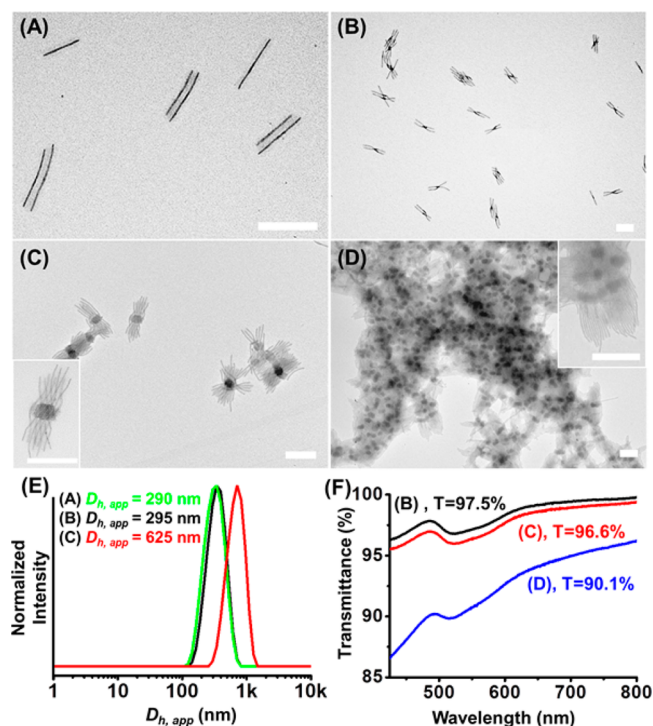


**Figure 4.** Typical TEM images of the structures formed by triblock comicelle P–H–P (A) individual cylinders ( $L_1 = 16$  nm,  $DP_2 = 600$ ); (B) multiple “cross” ( $L_1 = 56$  nm,  $DP_2 = 600$ ); (C) multiple “cross” plus bundles ( $L_1 = 56$  nm,  $DP_2 = 280$ ); and (D) bundles ( $L_1 = 56$  nm,  $DP_2 = 170$ ). Shown in image (E) are the normalized DLS data of the samples (A–C). Image (F) shows the transmittance data of sample (B–D). The origin of the very small (ca. 0.5%) reduction in transmittance at 520 nm in the spectra is unknown. Scale bars are 100 nm.

MeOH based on TEM observations and also DLS analysis. This strongly indicated that the aggregation of the triblock comicelles was indeed induced by the collapse of the PDMS chains, and that the PtBA chains in the neighboring segment serve only to provide colloidal stability.

**4. Construction of a Phase Diagram for Supermicelle Formation.** A total of 16 combinations of  $L_1$  (16, 27, 37, and 56 nm) and  $DP_2$  (170, 280, 460, 600) were explored. The TEM images of all the resulting assemblies from the 16 different combinations in MeOH after solvent evaporation are shown in Figure S2. With an increase of  $L_1$  from 16 to 56 nm, the hydrophobic effect became predominant, so that even with  $DP_2 = 600$  (corresponding to the largest coronal steric repulsion), the triblock comicelles were observed to aggregate and formed multiple “cross” supermicelles (Figure S2(D)). When the value of  $L_1$  was kept at 56 nm and  $DP_2$  was decreased to 170, the steric repulsion effect was reduced even further, and extremely large three-dimensional aggregates were formed (Figure S2(P)). TEM images of four typical supermicelles and their corresponding schematic representations are shown in Figure 5. Variation of  $L_1$  and  $DP_2$  clearly had a very significant influence on the structures of the supermicelles. A phase diagram is included in Figure 5(E) to summarize the supermicellar structures formed by these P–H–P amphiphilic triblock comicelles with the variation of  $L_1$  and  $DP_2$ . A general trend can be extracted from these images that the size of the supermicelles, or the number of triblock comicelles in each

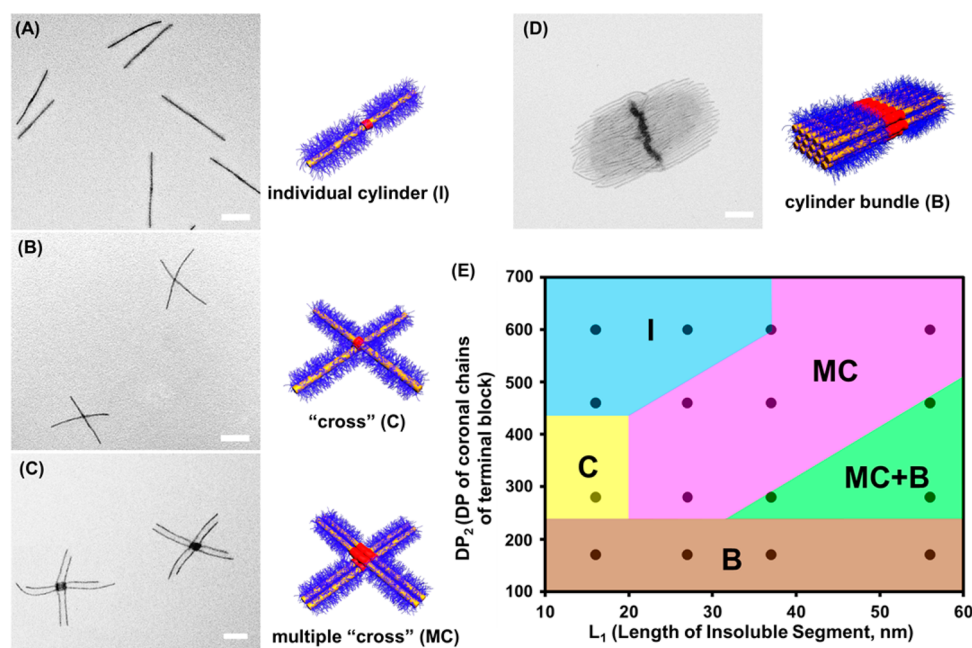


**Figure 5.** TEM images and the corresponding schematic representations of the structures formed in MeOH by the triblock comicelle P–H–P: (A) Individual cylinders ( $L_1 = 16$  nm,  $DP_2 = 600$ ), (B) “cross” micelles ( $L_1 = 16$  nm,  $DP_2 = 280$ ), (C) multiple “cross” micelles ( $L_1 = 27$  nm,  $DP_2 = 460$ ), and (D) a cylinder bundle ( $L_1 = 27$  nm,  $DP_2 = 170$ ) together with a simplified schematic representation to illustrate the packing. Scale bars are 200 nm. Shown in image (E) is the phase diagram summarizing the influences of  $L_1$  and  $DP_2$  (to which  $L_2$  is related, see SI pages 8–9 for details) on the supermicellar structures formed by the amphiphilic triblock comicelle P–H–P. Individual cylinders are marked as “I”, “cross” micelles as “C”, multiple “cross” as “MC” and cylinder bundles as “B”.

aggregate, increases with increasing values of  $L_1$  and decreasing values of  $DP_2$ .

**5. Generality of the Phase Diagram and the Predictable Formation of “Cross” Supermicelles.** To explore the generality of the phase diagram in Figure 5(E) we examined the self-assembly behavior of cylindrical triblock comicelles in which the P segments were replaced by M (PFS-*b*-P2VP) (P’ segments (P2VP = poly(2-vinylpyridine))). These P’–H–P’ triblock comicelles were also prepared via living CDSA using the 16 nm H seeds, and two PFS-*b*-P2VP polymers, PFS<sub>32</sub>-*b*-P2VP<sub>760</sub> and PFS<sub>25</sub>-*b*-P2VP<sub>250</sub> (Figure 6(A), Table S1). By analogy with the analysis of P–H–P block comicelles,  $L_2'$  is defined as the length of the P2VP chains, see Figure 6(B), but is represented in the following discussions by the degree of polymerization,  $DP_2'$ . Both examples of P’–H–P’ triblock comicelles were found to be dispersible in *n*-hexane : *i*-PrOH = 1:4 (Figure S4(A, B)). After dialysis against MeOH, no aggregation could be observed for triblock comicelles with  $DP_2' = 760$  (Figure S4(D)), while “cross” micelle formation was detected when  $DP_2' = 250$  (Figure 6(C)). These experimental results agreed well with our predictions based on the phase-diagram for P–H–P triblock comicelles (Figure 5(E)). Interestingly, when the P2VP chains of the P’–H–P’ ( $DP_2' = 250$ ) triblock comicelles were quaternized with  $CH_3I$ , the “cross” micelles were found to dissociate into individual cylinders based on TEM analysis (Figure 6(D)).

We further extended our studies to another triblock comicelle system in which both the terminal and the middle H segment were altered. The H segment was changed to M (PFS<sub>36</sub>-*b*-PMVS<sub>324</sub>) (PMVS = poly(vinylmethyl siloxane), H’) which, as expected, possessed similar solubility behavior to that of PDMS. Triblock comicelles P’–H’–P’ with  $L_1' = 20$  nm and  $DP_2' = 250$ , were prepared using living CDSA in a similar manner to the previous cases, using cylindrical H’ seeds with a

length of 20 nm. As shown in Figure 6(E), these triblock comicelles were also able to form “cross” micelles in pure MeOH. In addition, the terminal P’ blocks could be shell-cross-linked on the addition of Karstedt’s catalyst.<sup>15,19</sup> Both the vinyl groups on the PMVS chains and pyridyl groups on the P2VP chains were cross-linked (XL) (to give <sup>XL</sup>H’ and <sup>XL</sup>P’ segments, respectively)<sup>20</sup> and the whole supermicellar structure became permanently locked in. When THF (a good solvent for all the polymer blocks) was added into the solution with up to even 80% by volume, the “cross” <sup>XL</sup>P’-<sup>XL</sup>H’-<sup>XL</sup>P’ supermicelles were still stable, except that the cylinders appeared more curved and flexible, presumably due to the solvation of the previously rigid crystalline PFS core (Figure 6(F)). The experimental results on the P’–H–P’ and P’–H’–P’ systems clearly indicate that this phase-diagram has useful general applicability for different types of cylindrical triblock comicelles.

Atomic force microscopy (AFM) was also used to characterize the “cross” supermicelles shown in Figure 6(E). The AFM topographic image (Figure 6(G)) and the cross-sectional analysis (Figure 6(H)) of the “cross” supermicelles clearly revealed that they consist of two overlapping triblock comicelles.

**6. Characterization of “Cross” Supermicelles in Solution Using Laser Scanning Confocal Microscopy.** As discussed above (Section 3), an important issue concerns whether the “cross” supermicellar structures exist in the solution state or, instead, they are formed on solvent removal during sample preparation. To provide conclusive evidence, we labeled the supermicelles with a fluorescent dye and characterized them in solution by laser scanning confocal microscopy (LSCM, see SI pages 4–5). Dye labeling was accomplished by the addition of unimers of PFS<sub>20</sub>-*b*-PtBA<sub>320</sub>-D<sub>R</sub> (end-labeled with the red-dye, D<sub>R</sub>, BODIPY 630/650) to a solution of “cross” supermicelles (shown in Figure S5) that

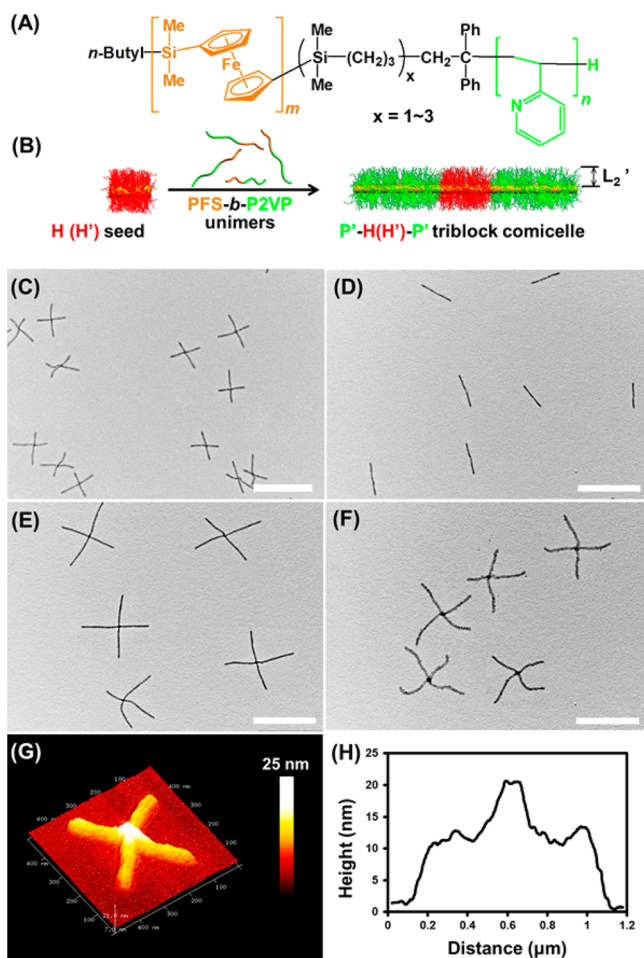


**Figure 6.** (A) Chemical structure of PFS-*b*-P2VP. (B) Schematic illustration of the living CDSA process to prepare a P'-H(H')-P' triblock comicelle and the definition of  $L_2'$ . (C-F) TEM images of triblock comicelles in MeOH after solvent evaporation (C) P'-H-P',  $DP_2' = 250$ ; (D) quaternized P'-H-P',  $DP_2' = 250$ ; (E) P'-H'-P',  $DP_2' = 250$ ; and (F)  $^{XL}P'-^{XL}H'-^{XL}P'$ ,  $DP_2' = 250$  triblock cylinder in MeOH: THF = 1:4.  $L_1 = 16$  nm in (C-D) and  $L_1' = 20$  nm in (E) and (F). Scale bars are  $1 \mu\text{m}$  in TEM images. Shown in (G) is the AFM topographic image of the "cross" supermicelles shown in image (E), and the cross-sectional analysis along one of the triblock comicelles is shown in (H).

were prepared from P'-H'-P' triblock comicelles (Figure 7(A)). The unimers added to the accessible PFS core termini of the "cross" supermicelles, and the length of the arms increased from  $210 \pm 20$  nm to  $2.5 \pm 0.2 \mu\text{m}$ , as shown by TEM analysis (Figure 7(B)). The resulting "cross" supermicelles could be readily observed by LSCM (Figure 7(C)).

To explore the robustness of these "cross" supermicelles, we further added a small amount of nonfluorescent PFS<sub>20</sub>-*b*-P2VP<sub>250</sub> unimers and subsequently the green dye-end-capped material PFS<sub>20</sub>-*b*-P2VP<sub>520</sub>-D<sub>G</sub> (D<sub>G</sub> = green-dye BODIPY FL) to the sample (Figure 7(E,F)). The length of the arms further increased to around  $5.9 \pm 0.3 \mu\text{m}$ , and the newly grown P' segment appeared to be darker in TEM images (Figure 7(E)), due to their long corona-chain length and higher electron density of P2VP relative to PtBA. The clear difference in the colors of the red-dye attached P segments and the green-dye attached P' segment demonstrated the successful preparation of "cross" block cosupermicelles and their existence in solution state (Figure 7(F)). Significantly, no detectable exchange

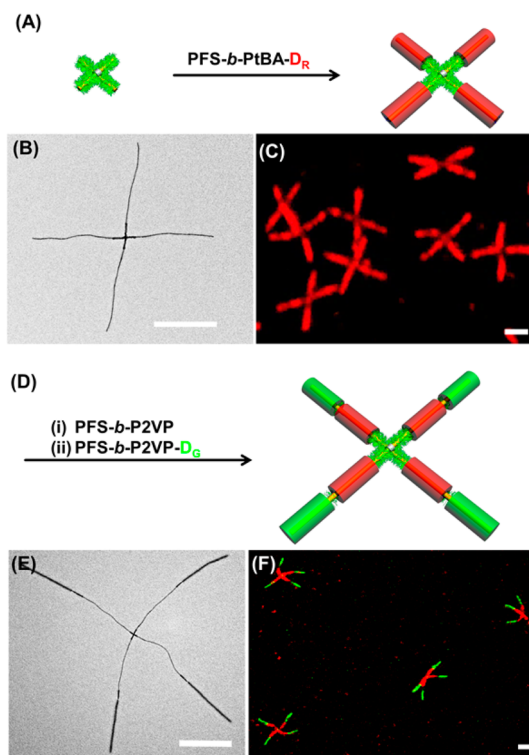


**Figure 7.** Schematic illustrations (A, D), TEM images (B, C) and LSCM images (in MeOH) (E, F) of block "cross" supermicelles prepared via the addition of fluorescent dye-containing unimers to the small "cross" micelles shown in Figure S5. Shown in (A-C) are the block "cross" supermicelles by adding PFS<sub>20</sub>-*b*-PtBA<sub>320</sub>-D<sub>R</sub>; and those shown in (D-F) are the blocky "cross" supermicelles by further adding nonfluorescent PFS<sub>20</sub>-*b*-P2VP<sub>250</sub> and PFS<sub>20</sub>-*b*-P2VP<sub>520</sub>-D<sub>G</sub>. Scale bars are  $2 \mu\text{m}$ .

between the red- and green-dye was observed after even 5 months of storage of these supermicelles. This indicated that the "cross" supermicelles are kinetically stable under these ambient temperature conditions on a time scale of several months.

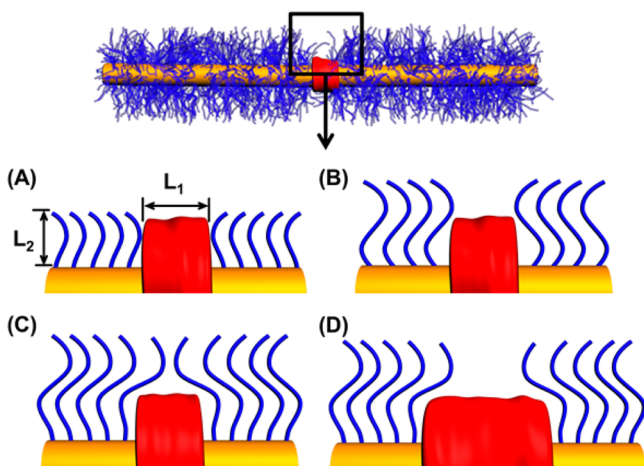
## DISCUSSION

### 1. Rationalization of the Accessible Morphologies from the Self-Assembly of Amphiphilic Cylindrical Triblock Comicelles.

The main factor influencing the aggregation behavior of the P-H-P triblock comicelle systems studied in this work is expected to be the balance between the interfacial energy of the collapsed PDMS chains of the supermicelle core with the solvent and the steric repulsions in the supermicelle corona between the PtBA chains (see Results, Section 1). As PDMS chains are insoluble in MeOH and collapse (Scheme 2), the strength of the hydrophobic interaction will increase with  $L_1$ , and this effect will promote aggregation of the triblock comicelles to form supermicelles. On the other hand, increasing  $L_2$  leads to increased steric hindrance, hindering triblock comicelle aggregation. As a further consideration, the long PtBA chains could partially cover the collapsed middle segments and reduce the interfacial energy. By manipulating the values of  $L_1$  and  $L_2$  (by means of  $DP_2$ ) different supermicellar aggregates or supermicelles were obtained.

When  $L_2$  is short ( $DP_2 = 170$ , see Scheme 2(A)), irrespective of the value of  $L_1$ , the triblock comicelles form bundles (see

### Scheme 2. The Influences of $L_1$ and $L_2$ on the Triblock Comicelles with a Hydrophobic Middle Segment with Collapsed Corona Chains<sup>a</sup>



<sup>a</sup>(A) Both  $L_1$  and  $L_2$  are small; (B)  $L_1$  is small and  $L_2$  is intermediate; (C)  $L_1$  is small and  $L_2$  is large; (D) both  $L_1$  and  $L_2$  are large.

Figure 5(E), brown “B” zone for bundles). This is presumably a consequence of the PtBA chains being insufficiently long to shield the collapsed PDMS chains from solvent, and thus the hydrophobic effect becomes predominant. This forces the triblock comicelles to minimize the interfacial energy via the preferential parallel aggregation of the hydrophobic H segments. Nevertheless, with an increasing value of  $L_1$  (and therefore an enhanced hydrophobic effect), the size of the bundles increases and the triblock comicelles aggregate in a less controlled manner (Figure S2).

When the value of  $L_2$  was intermediate ( $DP_2 = 280$ ) and  $L_1$  small ( $L_1 = 16$  nm), as shown in Scheme 2(B), the steric hindrance appears to become sufficient to preclude the possibility of parallel packing. Although the collapsed PDMS chains are probably partially shielded by the PtBA chains, particularly in the vicinity of the H–P block junctions, the triblock comicelles were found to aggregate. The resulting supermicelles possess middle segments oriented perpendicularly to each other, forming “cross” supermicelles (see Figure 5(E), yellow zone “C”). However, when the  $L_1$  value was increased, the steric hindrance is apparently insufficient to shield the collapsed PDMS chains and the triblock comicelles form multiple “cross” supermicelles (Figure 5(E), pink “MC” zone) and even bundles (Figure 5(E), green “MC+B” zone).

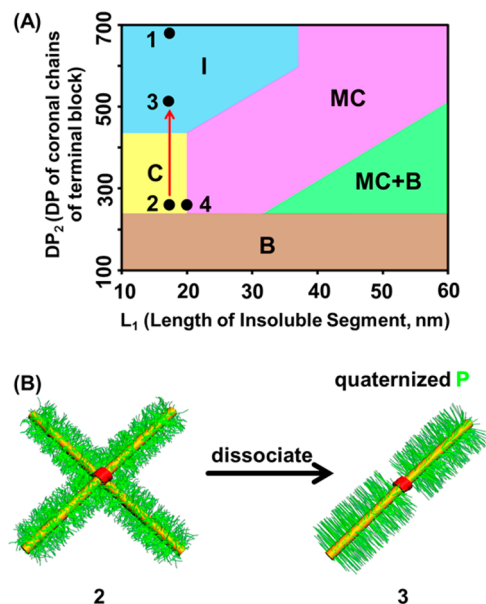
In contrast, in cases where the value  $L_2$  was large ( $DP_2 = 460$  and  $600$ ), and  $L_1$  small ( $L_1 = 16$  or  $27$  nm), only individual triblock comicelle cylinders were observed (see Figure 5(E), blue “I” zone for individual cylinders). The combination of a short H block and long PtBA chains hindered aggregation under these circumstances and it is likely that the PtBA chains in the P block could effectively shield the collapsed PDMS chains in the central H segment (Scheme 2(C)). On the other hand, when  $L_1$  was also large (Scheme 2(D)), the hydrophobic interactions were sufficient for aggregation to be detected and multiple “cross” supermicelles were formed (see Figure 5(E), pink “MC” zone).

**2. General Factors Favoring the Selective Formation of “Cross” Supermicelles.** As discussed above, for the P–H–P triblock comicelle building blocks, the structure of the resulting supermicelles can be qualitatively rationalized based

on the delicate energy balance arising from the interplay of  $L_1$  and  $L_2$ . Only when the value of  $L_1$  was sufficiently small ( $L_1$  near  $16$  nm) and  $L_2$  at an intermediate value ( $DP_2$  near  $280$ ), could “cross” supermicelles be formed (Figure 5(E)). Otherwise, with larger  $L_1$  or smaller  $L_2$  (i.e.,  $DP_2$ ) values, either multiple “cross” supermicelles were formed (via the aggregation of more than two triblock comicelles through their H segments due to the strong hydrophobic effect), or aggregation was prevented by steric hindrance, respectively (see Figure 5(E)). This indicates that “cross” micelles could only be formed under a specific set of conditions.

Although the conditions to produce “cross” supermicelles are presented for the P–H–P triblock comicelle system, we have also found it applicable to other, related block comicelle systems. For example, we explored P’–H–P’ triblock comicelles, where P2VP was used to replace PtBA as the terminal polar block. When the lengths of the P2VP blocks were characterized by  $DP_2'$  values of  $760$  and  $250$ , individual cylinders and “cross” supermicelles, were formed, respectively (Figure S4(D) and Figure 6(C)). Since the values of the characteristic ratio ( $C_\infty$ ) of PtBA ( $9.5$ ) and P2VP ( $9.6$ ) are very close,<sup>22</sup> it is reasonable to expect that the two kinds of polymers share similar volumes in MeOH. Thus, it is not surprising that the phase-diagram can also be applied to P’–H–P’ and P’–H’–P’ triblock comicelles. The supermicelles formed by the P’–H–P’ triblock comicelles are marked as Point 1 and 2 in Scheme 3(A), and both are located in the predicted zones, demonstrating the robustness of the phase-diagram.

### Scheme 3. (A) Experimental Results in the Phase-Diagram;<sup>a</sup> (B) Dissociation of “Cross” Supermicelles after Quaternization of the P2VP Chains on the P Segments



<sup>a</sup>The positions of these points are for illustration purpose and are more qualitative rather than quantitative.

When the P2VP corona ( $DP_2' = 250$ ) of the terminal P’ segments was quaternized with MeI, the resulting positively charged qP2VP chains stretch (as demonstrated by an increase of  $D_{h,app}$  for a P2VP homopolymer sample in MeOH: see SI page S8 for details). Thus, the value of  $L_2'$  should effectively increase even though the DP value of the P2VP block would be

unchanged.<sup>23</sup> Increased steric hindrance from the stretched qP2VP chains should hinder the aggregation of the triblock comicelles, ultimately leading to the dissociation of the “cross” supermicelles into individual cylinders (Figure 6 (D)) (Scheme 3(B)). Thus, in the phase-diagram shown in Scheme 3(A), the triblock comicelles might be considered to effectively move from point 2 in zone “C” to a position in zone “I” such as point 3 (chosen for illustrative purposes). However, electrostatic repulsions also likely play a key role in the dissociation of the cross micelles and these are not taken into account in the simple model used here.

Similarly, when P′–H′–P′ triblock comicelles were incorporated into the phase diagram, “cross” supermicelles should be formed (point 4 in Scheme 3(A)), and these were indeed observed by TEM (see Figure 6(E)). After cross-linking of the central H′ segments, the “cross” supermicelles were robust and stable even in the presence of a good solvent for the PFS core (Figure 6(F)). These observations demonstrate the relative robustness of the phase-diagram and highlight the conditions for producing “cross” supermicelles.

“Cross” supermicelles prepared in this work represent well-defined superstructures with uniform size and architecture (i.e., four arms with identical length) that are accessible from the hierarchical self-assembly of amphiphilic block comicelles. The approach that we have developed is a versatile method with which to produce these uniform superstructures in high yield, and their existence in solution state has been demonstrated by LSCM observations. The size of the “cross” supermicelles can be controlled from several hundred nanometers (Figure 5(B)) up to several micrometers (Figure 7(A–C)) simply by the addition of further unimers to the termini of the micelle cores at the ends of the arms. Furthermore, not only can the size be increased, but block cosupermicelles with segmented structures can be prepared by the addition of unimers derived from other PFS-containing BCPs. This is demonstrated by growing another green-dye-labeled PFS-*b*-P2VP-*D*<sub>G</sub> segment at the termini of these “cross” supermicelles, as shown in Figure 7(D–F).

## SUMMARY

An example of hierarchical assembly of amphiphilic BCP micelles into complex higher-level structures has been studied in detail. Monodisperse cylindrical block comicelles bearing hydrophobic central segments (H or H′) and polar end segments (P or P′) were prepared via living CDSA. The length and the positions of these segments were accurately controlled. The cylindrical block comicelles were assembled in polar solvents via hydrophobic interactions and various interesting and complex supermicellar structures were obtained. We focused on “cross” micelles and their formation can be rationalized by the influence of two factors: the hydrophobic interactions of the insoluble coronal block on the central H or H′ segment, and the steric repulsions from the soluble coronal block on the polar terminal P or P′ segment. A phase-diagram has been constructed based on the interplay of these two factors and the supermicellar structures observed and this allows the predictable formation of uniform “cross” supermicelles.

Although the methodology described here was based on PFS-containing BCPs and the use of organic media it should be extendable to aqueous systems and to the emerging group of other crystalline-coil BCPs and related amphiphiles that undergo seeded growth processes analogous to living

CDSA.<sup>21</sup> This should allow access to a variety of well-defined “cross” supermicellar structures with a wide range of functionality. The novel “cross” architectures accessible may be useful as models of biological structures such as chromosomes or as building blocks for the creation of yet more complex hierarchical materials using living CDSA from the core termini of the micelle arms.

## ASSOCIATED CONTENT

### Supporting Information

The Supporting Information is available free of charge on the ACS Publications website at DOI: 10.1021/jacs.5b12735.

Experimental details and additional results. (PDF)

## AUTHOR INFORMATION

### Corresponding Author

\*ian.manners@bristol.ac.uk

### Present Address

<sup>†</sup>Department of Polymer Materials, School of Material Science and Technology, Beijing Institute of Technology, Beijing 100081, PR China.

### Author Contributions

<sup>§</sup>X.L. and Y.G. contributed equally.

### Notes

The authors declare no competing financial interest.

## ACKNOWLEDGMENTS

X.L. acknowledges the EU for a Marie Curie Postdoctoral Fellowship. Y.G. and I.M. thank the EU for support. C.E.B. thanks the Bristol Chemical Synthesis Centre for Doctoral Training, funded by the Engineering and Physical Sciences Research Council, for a PhD studentship. M.A.W. thanks NSERC Canada for financial support. PeakForce atomic force microscopy was carried out in the Chemical Imaging Facility, University of Bristol with equipment funded by EPSRC under Grant “Atoms to Applications” Grant ref (EP/K035746/1). TEM studies were carried out in the Chemistry Imaging Facility at UoB with equipment funded by UoB and EPSRC (EP/K035746/1 and EP/M028216/1). The Ganesha X-ray scattering apparatus used for this research was purchased under EPSRC Grant “Atoms to Applications” Grant ref EP/K035746/1. We also thank the Wolfson Bioimaging Facility at the University of Bristol for the use of the confocal microscopy facilities.

## REFERENCES

- (1) (a) Palmer, L. C.; Stupp, S. I. *Acc. Chem. Res.* **2008**, *41*, 1674–1684. (b) Tadros, T. F. *Self-Organized Surfactant Structures*; Wiley-VCH: Weinheim, 2010. (c) Myers, D. *Surfactant Science and Technology*, 3rd ed.; Wiley: Hoboken, 2006.
- (2) (a) Mai, Y. Y.; Eisenberg, A. *Chem. Soc. Rev.* **2012**, *41*, 5969–5985. (b) Schacher, F. H.; Ruper, P. A.; Manners, I. *Angew. Chem., Int. Ed.* **2012**, *51*, 7898–7921.
- (3) (a) Zhang, L. F.; Eisenberg, A. *Science* **1995**, *268*, 1728–1731. (b) Pochan, D. J.; Chen, Z. Y.; Cui, H. G.; Hales, K.; Qi, K.; Wooley, K. L. *Science* **2004**, *306*, 94–97. (c) Cui, H. G.; Chen, Z. Y.; Zhong, S.; Wooley, K. L.; Pochan, D. J. *Science* **2007**, *317*, 647–650. (d) Zhu, J. H.; Zhang, S. Y.; Zhang, K.; Wang, X. J.; Mays, J. W.; Wooley, K. L.; Pochan, D. J. *Nat. Commun.* **2013**, *4*, 2297. (e) Dupont, J.; Liu, G.; Niihara, K.; Kimoto, R.; Jinnai, H. *Angew. Chem., Int. Ed.* **2009**, *48*, 6144–6147. (f) Li, Z. B.; Kesselman, E.; Talmon, Y.; Hillmyer, M. A.; Lodge, T. P. *Science* **2004**, *306*, 98–101. (g) Won, Y. Y.; Davis, H. T.; Bates, F. S. *Science* **1999**, *283*, 960–963. (h) Jain, S.; Bates, F. S. *Science*

- 2003, 300, 460–464. (i) Hayward, R. C.; Pochan, D. J. *Macromolecules* **2010**, *43*, 3577–3584. (j) Hu, X. L.; Hu, J. M.; Tian, J.; Ge, Z. S.; Zhang, G. Y.; Luo, K. F.; Liu, S. Y. *J. Am. Chem. Soc.* **2013**, *135*, 17617–17629. (k) Wang, X. R.; Hu, J. M.; Liu, G. H.; Tian, J.; Wang, H. J.; Gong, M.; Liu, S. Y. *J. Am. Chem. Soc.* **2015**, *137*, 15262–15275. (l) Rizis, G.; van de Ven, T. G. M.; Eisenberg, A. *Angew. Chem., Int. Ed.* **2014**, *53*, 9000–9003. (m) Ni, B.; Huang, M. J.; Chen, Z. R.; Chen, Y. C.; Hsu, C. H.; Li, Y. W.; Pochan, D.; Zhang, W. B.; Cheng, S. Z. D.; Dong, X. H. *J. Am. Chem. Soc.* **2015**, *137*, 1392–1395.
- (4) The assembly of amphiphilic nanoparticles is of broad interest. For examples of the hierarchical assembly of non-BCP based building blocks, see: (a) Zubarev, E. R.; Xu, J.; Sayyad, A.; Gibson, J. D. *J. Am. Chem. Soc.* **2006**, *128*, 15098–15099. (b) Zubarev, E. R.; Xu, J.; Sayyad, A.; Gibson, J. D. *J. Am. Chem. Soc.* **2006**, *128*, 4958–4959. (c) Pradhan, S.; Xu, L. P.; Chen, S. W. *Adv. Funct. Mater.* **2007**, *17*, 2385–2392. (d) Chen, Q.; Bae, S. C.; Granick, S. *Nature* **2011**, *469*, 381–384. (e) Chen, Q.; Whitmer, J. K.; Jiang, S.; Bae, S. C.; Luijten, E.; Granick, S. *Science* **2011**, *331*, 199–202.
- (5) Erhardt, R.; Zhang, M. F.; Böker, A.; Zettl, H.; Abetz, C.; Frederik, P.; Krausch, G.; Abetz, V.; Müller, A. H. E. *J. Am. Chem. Soc.* **2003**, *125*, 3260–3267.
- (6) (a) Gröschel, A. H.; Walther, A.; Löblich, T. I.; Schacher, F. H.; Schmalz, H.; Müller, A. H. E. *Nature* **2013**, *503*, 247–251. (b) Gröschel, A. H.; Schacher, F. H.; Schmalz, H.; Borisov, O. V.; Zhulina, E. B.; Walther, A.; Müller, A. H. E. *Nat. Commun.* **2012**, *3*, 710. (c) Fang, B.; Walther, A.; Wolf, A.; Xu, Y. Y.; Yuan, J. Y.; Müller, A. H. E. *Angew. Chem., Int. Ed.* **2009**, *48*, 2877–2880.
- (7) Nie, L.; Liu, S. Y.; Shen, W. M.; Chen, D. Y.; Jiang, M. *Angew. Chem., Int. Ed.* **2007**, *46*, 6321–6324.
- (8) Cheng, L.; Zhang, G.; Zhu, L.; Chen, D.; Jiang, M. *Angew. Chem., Int. Ed.* **2008**, *47*, 10171–10174.
- (9) (a) Zhang, K.; Fang, H.; Li, Z.; Ma, J.; Hohlbauch, S. V.; Taylor, J.-S. A.; Wooley, K. L. *Soft Matter* **2009**, *5*, 3585–3589. (b) Shrestha, R.; Elsbahy, M.; Luehmann, H.; Samarajewa, S.; Florez-Malaver, S.; Lee, N. S.; Welch, M. J.; Liu, Y. J.; Wooley, K. L. *J. Am. Chem. Soc.* **2012**, *134*, 17362–17365.
- (10) Liu, G. J.; Yan, X. H.; Li, Z.; Zhou, J. Y.; Duncan, S. J. *J. Am. Chem. Soc.* **2003**, *125*, 14039–14045.
- (11) (a) Rupar, P. A.; Chabanne, L.; Winnik, M. A.; Manners, I. *Science* **2012**, *337*, 559–562. (b) Qiu, H. B.; Russo, G.; Rupar, P. A.; Chabanne, L.; Winnik, M. A.; Manners, I. *Angew. Chem., Int. Ed.* **2012**, *51*, 11882–11885. (c) Qiu, H. B.; Hudson, Z. M.; Winnik, M. A.; Manners, I. *Science* **2015**, *347*, 1329–1332.
- (12) Living CDSA complements alternative routes to amphiphilic and patchy nanoparticles. See, for example, direct synthesis method: (a) Miyake, G. M.; Weitekamp, R. A.; Pionova, V. A.; Grubbs, R. H. *J. Am. Chem. Soc.* **2012**, *134*, 14249–14254. (b) Sveinbjornsson, B. R.; Weitekamp, R. A.; Miyake, G. M.; Xia, Y.; Atwater, H. A.; Grubbs, R. H. *Proc. Natl. Acad. Sci. U. S. A.* **2012**, *109*, 14332–14336. (c) Li, Z.; Ma, J.; Lee, N. S.; Wooley, K. L. *J. Am. Chem. Soc.* **2011**, *133*, 1228–1231. Film casting method: ref 5 and (d) Walther, A.; Andre, X.; Drechsler, M.; Abetz, V.; Müller, A. H. E. *J. Am. Chem. Soc.* **2007**, *129*, 6187–6198. (e) Walther, A.; Drechsler, M.; Rosenfeldt, S.; Harnau, L.; Ballauff, M.; Abetz, V.; Müller, A. H. E. *J. Am. Chem. Soc.* **2009**, *131*, 4720–4728. Solution self-assembly: ref 6 and (f) Voets, I. K.; de Keizer, A.; de Waard, P.; Frederik, P. M.; Bomans, P. H. H.; Schmalz, H.; Walther, A.; King, S. M.; Leermakers, F. A. M.; Stuart, M. A. C. *Angew. Chem., Int. Ed.* **2006**, *45*, 6673–6676. Emulsion method: (g) Nisisako, T.; Torii, T.; Takahashi, T.; Takizawa, Y. *Adv. Mater.* **2006**, *18*, 1152–1156. (h) Chen, C.-H.; Shah, R. K.; Abate, A. R.; Weitz, D. A. *Langmuir* **2009**, *25*, 4320–4323. Interfacial engineering method: ref 4c and (i) Liu, B.; Wei, W.; Qu, X. Z.; Yang, Z. H. *Angew. Chem., Int. Ed.* **2008**, *47*, 3973–3975. (j) Hong, L.; Jiang, S.; Granick, S. *Langmuir* **2006**, *22*, 9495–9499.
- (13) (a) Wang, X. S.; Guérin, G.; Wang, H.; Wang, Y. S.; Manners, I.; Winnik, M. A. *Science* **2007**, *317*, 644–647. (b) Gädt, T.; Jeong, N. S.; Cambridge, G.; Winnik, M. A.; Manners, I. *Nat. Mater.* **2009**, *8*, 144–150. (c) Gilroy, J. B.; Gädt, T.; Whittell, G. R.; Chabanne, L.; Mitchels, J. M.; Richardson, R. M.; Winnik, M. A.; Manners, I. *Nat. Chem.* **2010**, *2*, 566–570. (d) Hudson, Z. M.; Lunn, D. J.; Winnik, M. A.; Manners, I. *Nat. Commun.* **2014**, *5*, 3372. (e) Jia, L.; Zhao, G. Y.; Shi, W. Q.; Coombs, N.; Gourevich, I.; Walker, G. C.; Guérin, G.; Manners, I.; Winnik, M. A. *Nat. Commun.* **2014**, *5*, 3882. (f) Wang, H.; Patil, A. J.; Liu, K.; Petrov, S.; Mann, S.; Winnik, M. A.; Manners, I. *Adv. Mater.* **2009**, *21*, 1805–1808. (g) Hudson, Z. M.; Boott, C. E.; Robinson, M. E.; Rupar, P. A.; Winnik, M. A.; Manners, I. *Nat. Chem.* **2014**, *6*, 893–898.
- (14) Li, X. Y.; Gao, Y.; Boott, C. E.; Winnik, M. A.; Manners, I. *Nat. Commun.* **2015**, *6*, 8127.
- (15) (a) O'Reilly, R. K.; Hawker, C. J.; Wooley, K. L. *Chem. Soc. Rev.* **2006**, *35*, 1068–1083. (b) Thurmond, K. B.; Kowalewski, T.; Wooley, K. L. *J. Am. Chem. Soc.* **1996**, *118*, 7239–7240. (c) Guo, A.; Liu, G. J.; Tao, J. *Macromolecules* **1996**, *29*, 2487–2493.
- (16) (a) Ni, Y. Z.; Rulkens, R.; Manners, I. *J. Am. Chem. Soc.* **1996**, *118*, 4102–4114. (b) McGrath, N.; Schacher, F. H.; Qiu, H.; Mann, S.; Winnik, M. A.; Manners, I. *Polym. Chem.* **2014**, *5*, 1923–1929.
- (17) (a) Gilroy, J. B.; Rupar, P. A.; Whittell, G. R.; Chabanne, L.; Terrill, N. J.; Winnik, M. A.; Manners, I.; Richardson, R. M. *J. Am. Chem. Soc.* **2011**, *133*, 17056–17062. (b) Lammertink, R. G. H.; Hempenius, M. A.; Manners, I.; Vancso, G. J. *Macromolecules* **1998**, *31*, 795–800. (c) Papkov, V. S.; Gerasimov, M. V.; Dubovik, I.; Sharma, S.; Dementiev, V. V.; Pannell, K. H. *Macromolecules* **2000**, *33*, 7107–7115. (d) Chen, Z. H.; Foster, M. D.; Zhou, W. S.; Fong, H.; Reneker, D. H.; Resendes, R.; Manners, I. *Macromolecules* **2001**, *34*, 6156–6158.
- (18) (a) Hamley, I. W. *The Physics of Block Copolymers*; Oxford Science Publications: Oxford, 1998. (b) Hamley, I. W. *Introduction to Soft Matter*, 2nd ed.; J. Wiley: Chichester, 2007.
- (19) (a) Wang, X. S.; Arsenaault, A.; Ozin, G. A.; Winnik, M.; Manners, I. *J. Am. Chem. Soc.* **2003**, *125*, 12686–12687. (b) Wang, X. S.; Liu, K.; Arsenaault, A. C.; Rider, D. A.; Ozin, G. A.; Winnik, M. A.; Manners, I. *J. Am. Chem. Soc.* **2007**, *129*, 5630–5639. (c) Rupar, P. A.; Cambridge, G.; Winnik, M. A.; Manners, I. *J. Am. Chem. Soc.* **2011**, *133*, 16947–16957.
- (20) (a) Qiu, H.; Du, V. A.; Winnik, M. A.; Manners, I. *J. Am. Chem. Soc.* **2013**, *135*, 17739–17742. (b) Qiu, H.; Cambridge, G.; Winnik, M. A.; Manners, I. *J. Am. Chem. Soc.* **2013**, *135*, 12180–12183.
- (21) (a) Qian, J.; Li, X. Y.; Lunn, D. J.; Gwyther, J.; Hudson, Z. M.; Kynaston, E.; Rupar, P. A.; Winnik, M. A.; Manners, I. *J. Am. Chem. Soc.* **2014**, *136*, 4121–4124. (b) Patra, S. K.; Ahmed, R.; Whittell, G. R.; Lunn, D. J.; Dunphy, E. L.; Winnik, M. A.; Manners, I. *J. Am. Chem. Soc.* **2011**, *133*, 8842–8845. (c) Schmelz, J.; Schedl, A. E.; Steinlein, C.; Manners, I.; Schmalz, H. *J. Am. Chem. Soc.* **2012**, *134*, 14217–14225. (d) Gorl, D.; Zhang, X.; Stepanenko, V.; Würthner, F. *Nat. Commun.* **2015**, *6*, 7009. (e) Zhang, W.; Jin, W.; Fukushima, T.; Saeki, A.; Seki, S.; Aida, T. *Science* **2011**, *334*, 340–343. (f) Petzetakis, N.; Dove, A. P.; O'Reilly, R. K. *Chem. Sci.* **2011**, *2*, 955–960. (g) Robinson, M. E.; Lunn, D. J.; Nazemi, A.; Whittell, G. R.; De Cola, L.; Manners, I. *Chem. Commun.* **2015**, *51*, 15921–15924. (h) Rudolph, T.; von der Lühne, M.; Hartlieb, M.; Norsic, S.; Schubert, U. S.; Boisson, C.; D'Agosto, F.; Schacher, F. H. *ACS Nano* **2015**, *9*, 10085–10098. (i) Aliprandi, A.; Mauro, M.; De Cola, L. *Nat. Chem.* **2015**, *8*, 10–15. (j) Sun, L.; Pitto-Barry, A.; Kirby, N.; Schiller, T. L.; Sanchez, A. M.; Dyson, M. A.; Sloan, J.; Wilson, N. R.; O'Reilly, R. K.; Dove, A. P. *Nat. Commun.* **2014**, *5*, 5746.
- (22) (a) Xu, Z. D.; Hadjichristidis, N.; Fetters, L. J.; Mays, J. W. In *Physical Properties of Polymers*; Springer: Berlin, 1995. (b) *Polymer Handbook*; 4th ed.; Brandrup, J., Immergut, E. H., Grulke, E. A., Eds.; Wiley: New York, 1999.
- (23) (a) Thurmond, K. B.; Kowalewski, T.; Wooley, K. L. *J. Am. Chem. Soc.* **1997**, *119*, 6656–6665. (b) Guo, X.; Ballauf, M. *Langmuir* **2000**, *16*, 8719–8726.